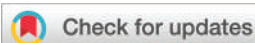


## PAPER

Cite this: *Nanoscale*, 2020, **12**, 6002

# Electrochemically addressable nanofluidic devices based on PET nanochannels modified with electropolymerized poly-*o*-aminophenol films†

Gregorio Laucirica,<sup>a</sup> Vanina M. Cayón,<sup>a</sup> Yamili Toum Terrones,<sup>a</sup> M. Lorena Cortez,<sup>a</sup> María Eugenia Toimil-Molares,<sup>b</sup> Christina Trautmann,<sup>b,c</sup> Waldemar A. Marmisollé<sup>\*a</sup> and Omar Azzaroni<sup>ID \*a</sup>

Nanofluidic field-effect transistors (nFETs) have attracted attention from the scientific community due to their remarkable level of control over ionic transport. Particularly, the combination of nanofluidic systems and electroactive polymers has demonstrated to be an interesting approach to achieve an electrochemically addressable device. In this work, the development of nFETs based on the integration of electropolymerized poly-*o*-aminophenol (POAP) films into track-etched nanochannels is proposed. The electropolymerization of POAP on the tip side of Au-sputtered asymmetric PET nanochannels not only allowed having a programmable tip diameter but also offered a precise and very rapid control of ionic transport by switching an external bias voltage. Moreover, the system exhibited a reversible behaviour between non-selective and anion-selective states. We believe that this work provides new tools and concepts to design and build high-performance nanofluidic field-effect transistors working under electrochemically controlled conditions.

Received 6th December 2019,

Accepted 7th February 2020

DOI: 10.1039/c9nr10336h

rsc.li/nanoscale

## Introduction

Biological ionic channels are transmembrane proteins that allow an ionic flux between a cell and its external medium.<sup>1</sup> Up to now, a wide variety of ionic channels with different features are known. Despite the broad spectrum of biological channels, most of them have some common important properties such as, for example, ionic selectivity and stimulus-responsiveness.<sup>2</sup> Thereby, channels able to trigger a response (*i.e.*: signal) in the presence of a certain stimulus as, for example, an external electric field or changes in some ligand concentrations, endow the channel with the desirable feature of stimulus-responsiveness. The fascinating properties of biological ionic channels have inspired the design of abiotic nanopores (solid-state nanochannels, SSNs) using materials

that provide versatility, robustness and resistance to different environmental conditions together with a precise ionic flux control.<sup>3–6</sup>

Particularly, the development of SSNs in polymer membranes by the ion-track-etching technique has attracted special attention due to several reasons.<sup>7</sup> Firstly, the channel surface obtained by this technique exhibits carboxylate groups that produce, under suitable conditions, charged surfaces allowing both its operation as an ionic filter and subsequent surface modifications.<sup>8,9</sup> Moreover, this method allows the development of nanochannels with tailored geometries.<sup>10–13</sup> The rupture of electrical potential introduced by asymmetric shapes is crucial as it leads to the development of devices with ionic current rectification (ICR).<sup>14</sup> The ICR implies that the current is favoured in a certain polarity of transmembrane voltage over the reverse polarity, *i.e.* there is a diode-like charge transport. This phenomenon has been used in several applications such as biosensing, and the development of ionic diodes and ionic filters, among others.<sup>9,15–17</sup> Alternatively, asymmetric current flows can also be achieved by asymmetric surface modifications and even by heterogeneous surface charge distributions.<sup>18</sup>

To imitate the biological counterpart, researchers have shown great interest in the development of devices with ionic fluxes that are subjected to external and non-invasive stimuli. In this sense, SSNs responsive to a wide variety of stimuli such

<sup>a</sup>Instituto de Investigaciones Fisicoquímicas Teóricas y Aplicadas (INIFTA), Departamento de Química, Facultad de Ciencias Exactas, Universidad Nacional de La Plata, CONICET – CC 16 Suc. 4, 1900 La Plata, Argentina.

E-mail: azzaroni@inifta.unlp.edu.ar, wmarmi@inifta.unlp.edu.ar; <http://softmatter.quimica.unlp.edu.ar>, [www.twitter.com/softmatterlab](http://www.twitter.com/softmatterlab), [www.facebook.com/SoftMatterLaboratory](http://www.facebook.com/SoftMatterLaboratory)

<sup>b</sup>GSI Helmholtzzentrum für Schwerionenforschung, 64291 Darmstadt, Germany

<sup>c</sup>Technische Universität Darmstadt, Materialwissenschaft, 64287 Darmstadt, Germany

†Electronic supplementary information (ESI) available. See DOI: 10.1039/c9nr10336h

as light, temperature, pH and chemical effectors have been designed.<sup>19–22</sup> In this regard, the application of a bias voltage as a non-invasive effector in order to control the ionic flux through the SSN emerges as an interesting option.<sup>23</sup> Given the similarities between these systems and the field-effect transistor (FET), these devices can be referred to as nanofluidic field-effect transistors (nFETs) and the bias voltage can be considered as the gate voltage ( $V_g$ ) in traditional FETs.

Over the last few years, researchers have attained to control ionic transport by means of  $V_g$  using different strategies. Within the field of two-dimensional nanofluidic devices, over the last few years voltage-gated responses have been achieved by a variety of configurations and materials,<sup>24</sup> such as graphene<sup>25,26</sup> and graphene oxide stack membranes<sup>27</sup> and more recently by the laminar assembly of Mxenes.<sup>28</sup> Concerning the ionic transport through nanochannels in polymer membranes, seminal studies of Martin *et al.* on Au nanotubule membranes showed that the application of a  $V_g$  allows the control of the excess Au surface charge and this fact produces a direct effect on the ionic transport of ions through the nanotubule.<sup>29</sup> At the beginning, the voltage-gated transport in track-etched membranes was achieved by means of successive deposition of semiconductor and metal layers onto polymer foils.<sup>30</sup> Recently, a new generation of nFETs was introduced, where the successive semiconductor depositions were replaced by the controlled growing of electroactive polymer layers.<sup>31–33</sup> Added for the ease of preparation, these systems opened the floodgates to the design of a wide variety of arrays by exploiting the interesting attributes of electroactive polymers.<sup>34–36</sup> Nevertheless, despite the advantages exhibited by nFETs based on electroactive polymers, their study remains scarce. In this context, it is necessary to continue exploring the rational design and synthesis of nFET devices which exhibit favourable features such as robustness, reproducibility, and quick response, among others.

Electroactive polymers are polymers that can be reversibly oxidized or reduced by means of, for example, the application of a bias voltage.<sup>37,38</sup> Moreover, taking into account their electron-transport mode, these polymers can be classified into two groups: electronically conducting polymers (CPs) and redox polymers (RPs). On one side, RPs contain redox sites electrostatically or covalently attached to the polymer structure, such as in the case of poly-(vinylferrocene) and quinone-polymers. The electron transport in these systems is carried out by electron hopping. On the other hand, the CP structure is constituted by double bound conjugated chains, which allows charge conduction along the polymer. Among the whole family of CPs, polypyrrole (PPy), poly(3,4-ethylenediothiophene) (PEDOT) and polyaniline (PANI) are the most archetypal examples. Within this last group, PANI has been one of the most studied polymers. The robustness and chemical stability of PANI has positioned it as a good candidate for the development of biosensors, supercapacitors, electrochromic devices, and batteries, among other applications.<sup>39–42</sup> The extraordinary properties of PANI encouraged researchers to synthesize polymers based on substituted anilines such as poly(*o*-amino-

phenol) (POAP).<sup>43,44</sup> POAP is a widely studied polymer synthesized from *ortho*-aminophenol (*o*-AP).<sup>45–47</sup> However, unlike aniline, *o*-AP polymerization provides a redox-type polymer, with two redox states (Fig. 1). Moreover, the chemical nature of quinone redox couples confers the POAP films with a high permselectivity.<sup>48,49</sup> These characteristics turn POAP into a good candidate for the development of smart SSN-based platforms with voltage-gated selectivity.

In this work, we present the development of a voltage-gated nanofluidic diode based on the electrochemical polymerization of *o*-AP in asymmetric gold-coated polyethylene terephthalate (PET) single nanochannels. Particularly, we show that the site-selective electrosynthesis of POAP at the small opening (*i.e.*: the tip) of the nanochannel confers the properties of ionic current rectification to the nanofluidic device. We found that external gate voltages applied to the device can be used to control the redox state of the polymer in the nanochannel and, consequently, to dictate its ion transport and current rectification properties. We believe that the reversible redox characteristics offered by POAP films in combination with the remarkable physical characteristics of asymmetric nanopores constitute a new framework for the design of multifunctional nanofluidic devices employing external voltages as the non-invasive stimulus to trigger a predefined iontronic response.

## Results and discussion

First, bullet-shaped single nanochannels in PET foils (12  $\mu\text{m}$  thickness) were fabricated by the ion-track-etching method.<sup>7</sup> For this purpose, the foils were irradiated with a single swift heavy ion and subsequently exposed to a chemical etchant. Thus, asymmetric bullet channels were obtained by surfactant-assisted etching.<sup>50</sup> Then, the foils were coated with a gold layer ( $\sim 80$  nm) on the tip side *via* sputtering. This method led to nanochannels with small opening diameters ( $d_{\text{tip}}$ ) of  $\sim 80$  nm and base diameters ( $D$ ) of  $\sim 650$  nm (Fig. S1†). The Au-coated side on the membranes was then modified with a POAP layer by electropolymerization.

As reported by Tucceri, *ortho*-amino-phenol (*o*-AP) can be polymerized electrochemically in acidic, neutral and alkaline solutions.<sup>46</sup> However, whereas an electroactive film is formed in acidic media, POAP films synthesized in neutral and alkaline media present no electroactivity.<sup>46</sup> Therefore, the metallized foils were modified by *in situ* electropolymerization of *o*-AP according to the experimental conditions described by Barbero *et al.*<sup>51</sup> Electrosynthesis was carried out by cyclic voltammetry in acidic medium (2 mM *o*-AP in 0.1 M  $\text{HClO}_4$ /0.4 M  $\text{NaClO}_4$ , pH  $\sim 1$ ) using a classical three-electrode array in which the gold-sputtered membrane was used as the working electrode. The metallized membrane was subjected to subsequent potential scans (see the ESI†) for depositing a film of the electroactive polymer onto the side of the nanochannel tip.

The mechanism of electro-oxidation of *o*-AP involves different chemical steps (Fig. 1(a)).<sup>51</sup> In Fig. 1(b), voltammo-

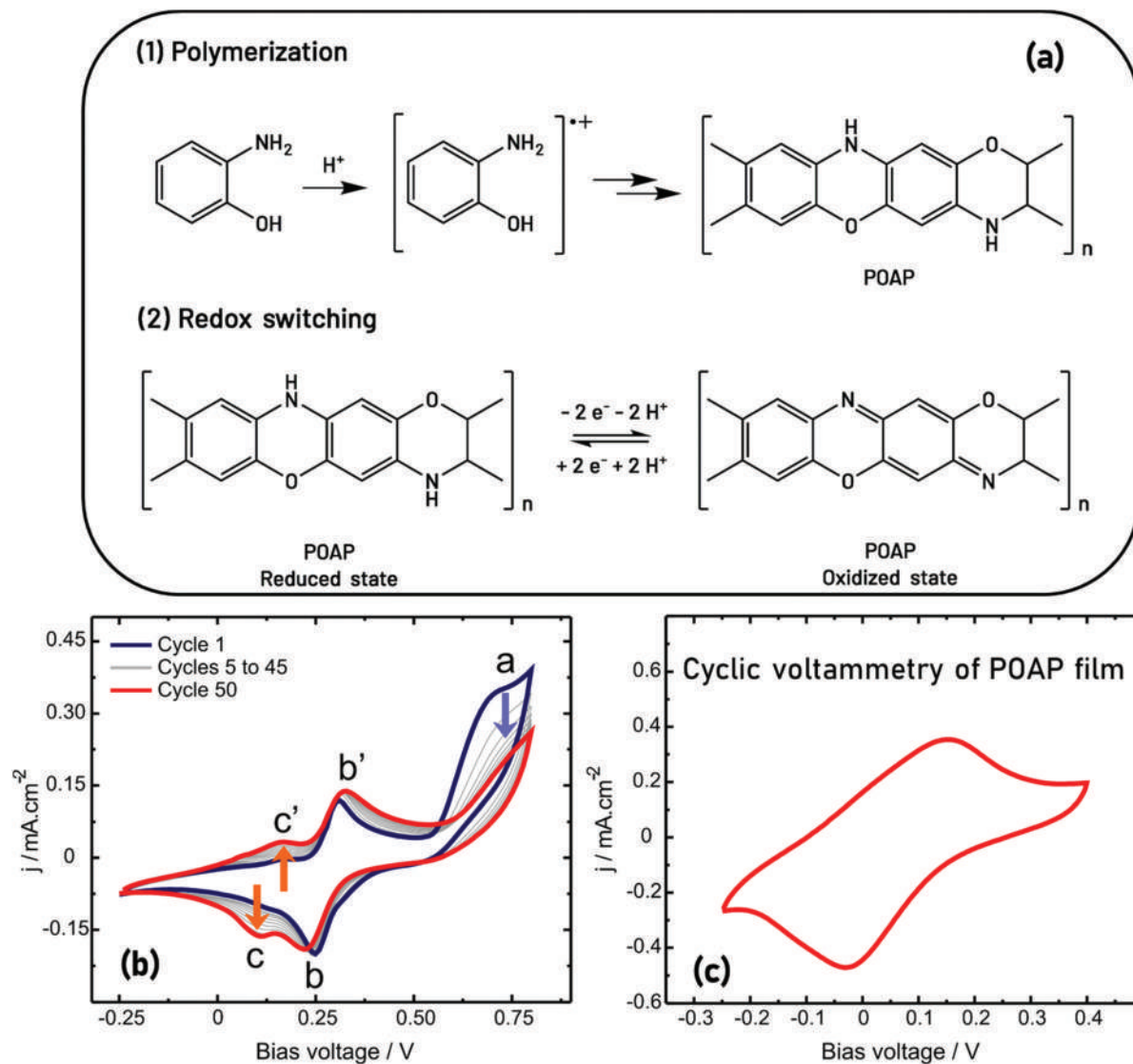


**Fig. 1** (a) Reaction schemes: (1) POAP formation reaction from *o*-AP and (2) POAP redox switching; (b) voltammograms for the synthesis of POAP at different steps of the electropolymerization: at the beginning (blue, 1st cycle), between 5th and 45th cycles (grey, recorded every 5 cycles) and the last one of 50 cycles (red) (2 mM *o*-AP in 0.1 M  $\text{HClO}_4$ /0.4 M  $\text{NaClO}_4$ , pH  $\sim$  1); (c) cyclic voltammetry of the final POAP polymer film deposited onto the tip side of the Au-sputtered foil (0.01 M  $\text{HClO}_4$ /0.04 M  $\text{NaClO}_4$ , pH  $\sim$  2).

grams for the synthesis of POAP at different stages (*i.e.*: number of voltammetric cycles) of the electropolymerization are shown. On the first positive sweep, a broad peak, **a**, can be noticed in the region of 0.7–0.75 V due to the oxidation of *o*-AP to a monocation radical ( $o\text{-AP}^{\cdot+}$ ) and then to a dication radical ( $o\text{-AP}^{2+}$ ). On the negative sweep, this broad peak does not show a complementary one, indicating chemical follow-up reactions giving products detected as peaks **b–b'** and **c–c'** on the subsequent sweeps. The peak system **c–c'** increases on cycling, showing the characteristic behaviour of a deposited electroactive substance, *i.e.* the formation of the POAP film.<sup>46</sup> The overall polymer formation reaction is depicted in Fig. 1(a).

The cyclic voltammetry results of the POAP film deposited into the tip side of the nanochannel are shown in Fig. 1(c). Thereby, these voltammograms reveal the redox switching of

POAP (Fig. 1(a)) in acidic media that arises from the deposited electroactive POAP film. Unlike other electroactive polymers based on substituted aniline, the voltammetric wave is characterized for only one redox reaction carried out at bias voltages of  $\sim$ 0–0.1 V vs. Ag/AgCl.<sup>21,44</sup> Specifically, the redox couple is centred at  $\sim$ 65 mV at pH = 1 which is in good agreement with the previously reported values.<sup>46,51</sup> Furthermore, a POAP film thickness of  $\sim$ 25–30 nm could be estimated by the voltammetric charge that comes from the reduction peak (see ref. 43 for further details).

The voltammogram in Fig. 1(c) is not symmetric, suggesting a complex redox behaviour that does not follow the simple Nernstian model (further details about the electrochemical behaviour of POAP are available in ESI, Fig. S2†).<sup>46</sup> Previous studies have demonstrated that variables, such as film thick-

ness, solution pH and redox couple concentrations in solution, affect both the permeation process of electroactive species and the electron motion through a POAP film.<sup>52–54</sup>

The identity of the polymer film was confirmed by Raman spectroscopy. The results in Fig. 2(a) indicate that the *c-c'* couple belongs to a phenoxazine-like chain structure of POAP, in accordance with previously published results.<sup>51,52,54</sup> Compared to the bare PET/Au surface, the region around 1100–1700  $\text{cm}^{-1}$  shows the typical bands of arylamine-based polymers.<sup>19,53</sup> More specifically, the outstanding signals associated with POAP are: C–H bending in plane (1170  $\text{cm}^{-1}$ ),  $-\text{C}-\text{N}^+$  radical semiquinone (1325  $\text{cm}^{-1}$ ),  $-\text{C}=\text{N}-$  quinoid ring (1475  $\text{cm}^{-1}$ ) and  $\text{C}=\text{C}-$  aromatic ring (1500  $\text{cm}^{-1}$ ) stretching vibrations. Also, the spectrum shows the band corresponding to the benzenoid ring deformation at 570  $\text{cm}^{-1}$ .<sup>55</sup>

Surface wettability changes were determined by contact angle measurements as shown in Fig. 2(b). Several studies have proved the influence of wettability on the ionic transport.<sup>34,56,57</sup> For this reason, the contact angle changes of the Au-coated foil were studied before and after the modification with POAP. Thus, the contact angle values determined with 0.01 M  $\text{HClO}_4$ /0.04 M  $\text{NaClO}_4$  solution were  $\sim 65^\circ$  and  $\sim 30^\circ$  before and after the polymerization, respectively. The marked increase in the hydrophilicity confirms the functionalization with POAP.

In order to study the iontronic behavior of the nanochannel, *I-V* curves before and after the electrodeposition of POAP were recorded using a four-electrode arrangement (Fig. S3†). Conductometric measurements carried out on the Au-coated foil (PET/Au) showed a cation-selective rectified transport, whose selectivity is ascribed to the negative surface charge of the gold layer caused by the adsorption of perchlorate ions (Fig. 3(a) and (b)). As previously reported, the rectification effect arises from the disruption of the symmetry in the electric potential along the nanochannels,<sup>13</sup> and perm-selectivity

towards a certain type of ion stems from the interaction between mobile ions and surface charged groups in the tip region.<sup>58</sup> Also, the rectification behaviour is highly dependent on factors such as the surface charge, the nanometric size of the nanochannel, the ionic strength, and the presence of specific ionic moieties, among others.<sup>4,59–61</sup>

After the deposition of POAP, the nanochannel presents a different iontronic response (Fig. 3(b)). More specifically, after functionalization with POAP, the device showed an ohmic response under high ionic strength acidic conditions. This behaviour suggests that the as-synthesized polymer has a low charge state which, in solutions of high ionic strength, produces the loss of ICR effect. Moreover, a concomitant decrease in transmembrane currents evidences a reduction in the size of  $d_{\text{tip}}$  after the POAP modification (Fig. 3(d)). As shown in Fig. 3(d), the effective tip diameter estimated from the nanochannel conductance decreases with the number of voltammetric cycles during the electropolymerization of POAP (for further details see the ESI†). These results are in accordance with the previously reported studies on nanochannels modified with other electrochemically active polymers.<sup>21,32</sup> In this regard, electropolymerization on metallized PET nanochannels constitutes a very promising bottom-up strategy to develop rectifying nFETs, due to the precise control on the film thickness and, thus, the possibility of selectively changing the effective tip diameter.

As previously mentioned, POAP is an electroactive polymer formed by phenoxazine units that act as redox centers. Thus, by applying suitable bias voltage, the electroactive polymer can alternate between reduced ( $\text{POAP}_{(\text{red})}$ ) and oxidized ( $\text{POAP}_{(\text{ox})}$ ) states.<sup>46,51</sup> The reduced state is rich in amine groups whereas the oxidized state is characterized by the presence of imine groups. The redox behaviour of POAP has been extensively studied by several groups.<sup>55,62–66</sup> In particular, it has been reported that the voltammetric response of POAP films strongly depends on pH. The voltammograms are ill-defined

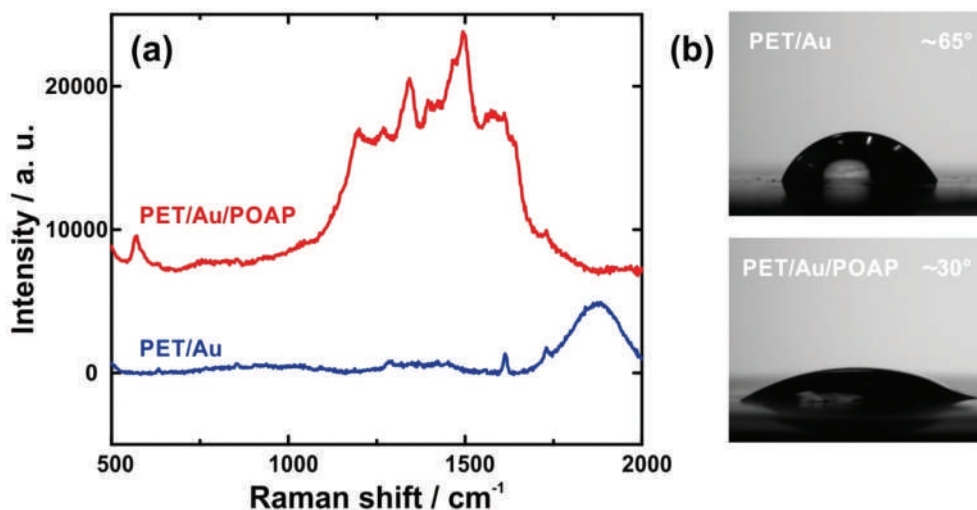
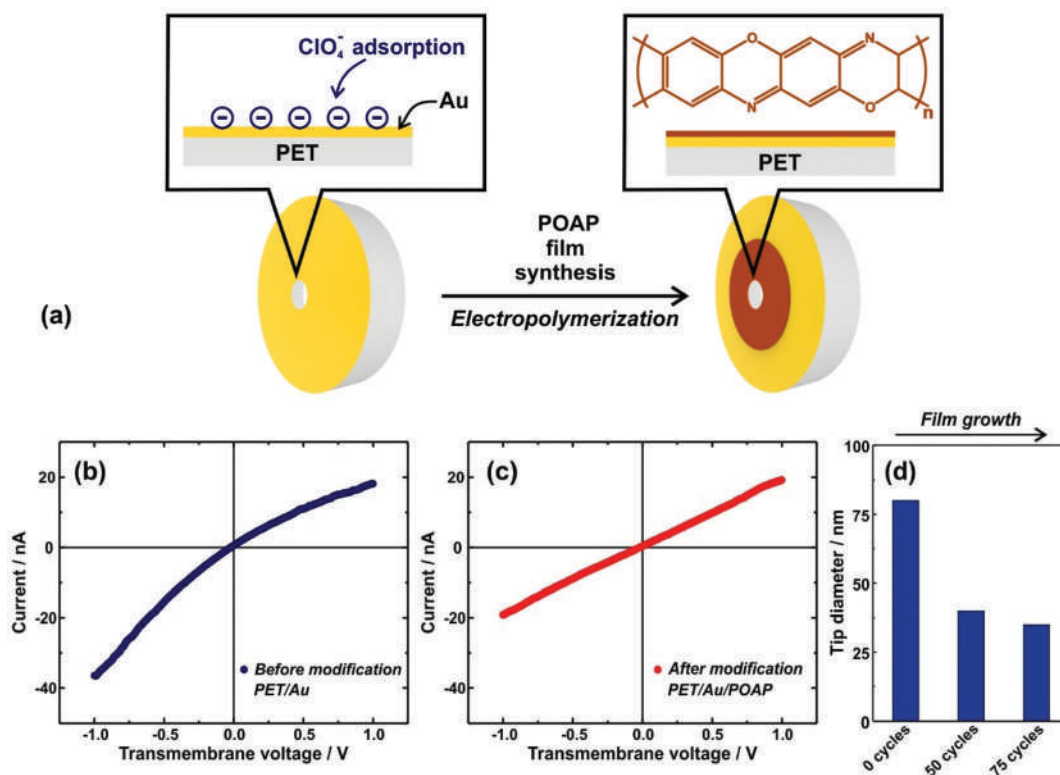
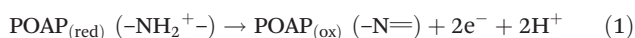


Fig. 2 (a) Raman spectra of the Au-sputtered PET membrane before and after o-AP electropolymerization; (b) contact angle before and after the POAP modification. All measurements were carried out with a 10 mM  $\text{HClO}_4$ –40 mM  $\text{NaClO}_4$  solution.



**Fig. 3** (a) Schematic representation of the electrochemical polymerization of *o*-AP onto the metallized PET membrane containing the bullet-shaped nanopore; *I*-*V* curves ( $\text{HClO}_4$  0.1 M +  $\text{NaClO}_4$  0.4 M): (b) before (blue) and (c) after the electropolymerization (red). (d) Tip diameters obtained after different electropolymerization cycles of *o*-AP. The increase in the number of electropolymerization cycles produces an increase in the film thickness with a concomitant decrease in the tip diameter.

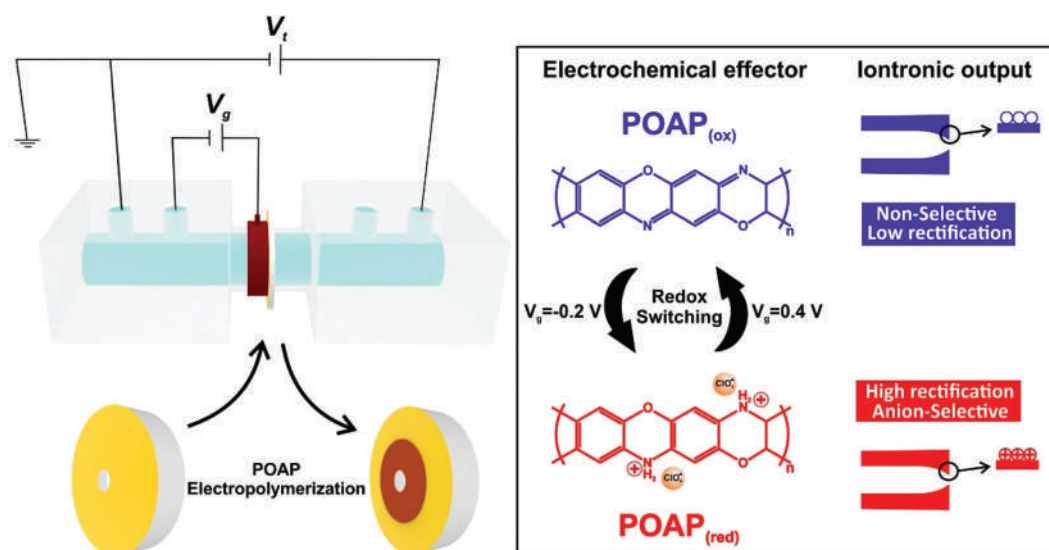
for pH higher than 3 and for pH close to 5 the cathodic peak practically disappears.<sup>53,63</sup> Furthermore, it has been proposed that the redox mechanism in acidic media is complex involving both the addition and elimination of protons.<sup>63</sup> The oxidation of  $\text{POAP}_{(\text{red})}$  is a two-electron process coupled to the release of two protons. It requires the amine groups in  $\text{POAP}_{(\text{red})}$  to be protonated and yields non-protonated imine moieties. Thus, the whole process taking place at pH lower than 3 can be depicted as



The  $\text{p}K_{\text{a}}$  value for the reduced form of POAP has been estimated to be about 2.5.<sup>46,63</sup> Then, at pH lower than 2.5, a high proportion of the amine groups are protonated in  $\text{POAP}_{(\text{red})}$ .<sup>53</sup> In contrast, the imine groups remain unprotonated even at this highly acidic pH. As a result, the redox conversion of POAP at pH lower than 2.5 implies a net change in the polymer ionic charge from positive in the reduced state to nearly neutral in the oxidized form. Taking into account the marked influence of the surface charge on the ionic transport in nanochannels, the integration of POAP onto the tip side of the nanochannel would produce redox responsiveness to the nanofluidic device, allowing the modulation of the iontronic response by the application of suitable redox potential values

to the membrane (gate voltages) (Scheme 1). Moreover, the use of highly acidic solutions (pH 1–2) would allow guaranteeing both the reversibility of the POAP redox switching and the differential protonation of the reduced and oxidized forms. Nanofluidic devices operating under such highly acidic conditions have been rarely reported, so the integration of POAP to SSNs may potentially offer new insights into harsh environment gating applications.

In order to control the POAP redox state and to simultaneously record the iontronic output, a bipotentiostat set-up was used (Fig. S3†). Hence, a potentiostat connected in a three-electrode arrangement was used to control the applied potential to the Au-coated foil, connected to an external Cu ring. This allowed, in a first step, the synthesis of the electroactive polymer film on the tip side by means of the electropolymerization of monomer *o*-AP by cyclic voltammetry. The same three electrode configuration was then employed to control the POAP redox state through the application of certain potential during the transmembrane measurements. In line with the FET analogy, this potential applied to the membrane is also referred to as the gate voltage ( $V_{\text{g}}$ ). Simultaneously, the iontronic response was recorded with another potentiostat set-up connected to a four-electrode array. Scheme 1 depicts a simplified electrode configuration; further details are presented in the ESI.†



**Scheme 1** Scheme of the cell used for POAP nFET measurements (left). The relation between the gate voltage, redox state and the iontronic output for the POAP functionalized nanochannel is presented (right).

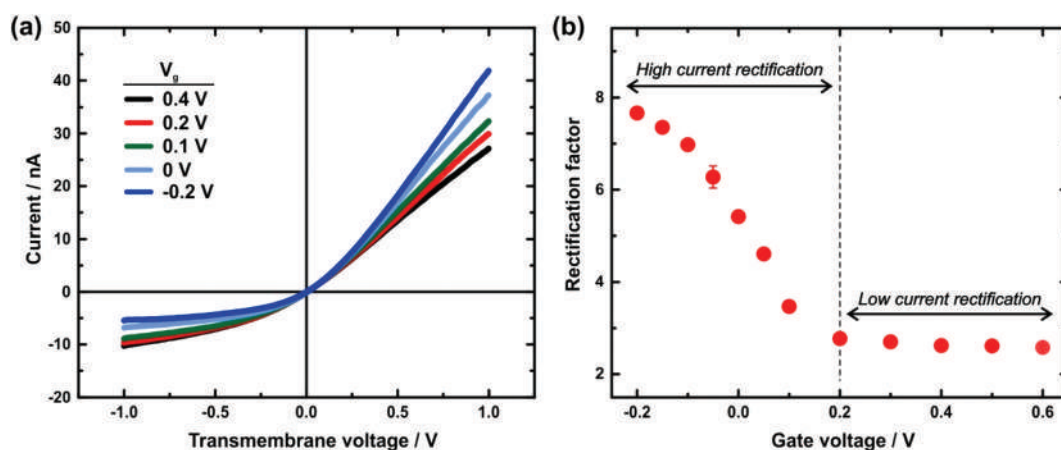


**Fig. 4** (a)  $I$ - $V$  curves of the PET/Au/POAP nanochannel at different values of the gate voltage; (b) rectification factors obtained from the  $I$ - $V$  curves as a function of the gate voltage. All measurements were carried out in a 10 mM  $\text{HClO}_4$  + 40 mM  $\text{NaClO}_4$  aqueous solution.

Fig. 4 shows the  $I$ - $V$  curves recorded at different values of the redox potential applied to the membrane. In agreement with the voltammetric response, the iontronic output showed an appreciable influence of  $V_g$  for values around 0.2 V (Fig. 4(a)). For  $V_g > 0.2$  V, the  $I$ - $V$  curves show a quasi-ohmic behaviour, *i.e.* a low ICR ascribed to the low charge state of POAP<sub>(ox)</sub>. However, for  $V_g < 0.2$  V, an enhancement of anion-driven rectification was triggered caused by the electrochemical reduction of the POAP film. Appropriate control experiments show that the same iontronic behaviour is obtained when PET/Au membranes are subjected to different  $V_g$  values, whereas clear gating effects are obtained after depositing the POAP layer on the same membrane, supporting the idea that  $V_g$  causes a change in the iontronic response due to the presence of the POAP film (Fig. S4†).

The ICR mechanism has been explained using different models.<sup>14,67–69</sup> PNP simulations have revealed that the surface charge produces the accumulation or depletion of ions in the tip region depending on the applied transmembrane voltage,  $V_t$ .<sup>58,67</sup> Particularly in the present system, when  $V_g$  is fixed at a value lower than 0.2 V, POAP acquires positive charge due to the reduction of imine groups to charged amine groups. This increment in the surface charge in the nanochannel tip region triggers an enhancement of the ionic rectification. Therefore, the behavior of iontronic output implies that the system can be switched from low-rectification to anion-driven rectification by means of the application of very low gate voltages ( $-0.2$  V  $<$   $V_g$   $<$  0.2 V). Moreover, it is important to emphasize that the system showed good stability in the current measurements (Fig. S5†).

With the aim of quantifying the ICR efficiency of the iontronic response, the rectification factor ( $f_{\text{rec}}$ ) was used. This parameter is calculated as a ratio between the currents at  $\pm 1$  V (see the Experimental section). The previously reported studies have demonstrated that  $f_{\text{rec}}$  is very sensitive to changes in the surface charge as well as in ionic strength, channel diameter and geometry, among others.<sup>4,70–74</sup> Nevertheless, taking into account the experimental conditions used in this work, we are able to ascribe changes in  $f_{\text{rec}}$  to changes in the POAP surface charge. Fig. 4(b) shows the influence of  $V_g$  on the ionic transport in terms of  $f_{\text{rec}}$ . When  $V_g > 0.2$  V, the iontronic output exhibited a low  $f_{\text{rec}}$ , between 2 and 3. This behaviour must be due to the low charge state of POAP<sub>(ox)</sub> and can be correlated to a low ionic selectivity.<sup>58</sup> On the other hand, when  $V_g < 0.2$  V,  $f_{\text{rec}}$  increased markedly and became even larger as  $V_g$  decreased, in line with the electrochemical reduction of POAP<sub>(ox)</sub> to the protonated POAP<sub>(red)</sub>. The study of the influence of pH on the iontronic response of POAP-modified membranes at  $V_g = -0.2$  V (Fig. S6†), allowed the confirmation of the proposed acid–base behaviour for the reduced form of POAP. The analysis in terms of  $f_{\text{rec}}$  gives an effective  $\text{p}K_a$  value of 2.4 for this redox form, which is in excellent agreement with the estimated value from electrochemical results.<sup>46,63,66</sup> Hence, in acidic media, unprotonated imine groups in POAP<sub>(ox)</sub> are reduced to protonated amine groups in POAP<sub>(red)</sub> and, therefore, a net number of positively charged sites are produced in the film upon electrochemical reduction.<sup>53,63,75</sup> To evaluate the effect of the presumed hydrophobicity change caused by the gate voltage on the iontronic response, the influence of  $V_g$  on the contact angle of drops of 10 mM HClO<sub>4</sub> + 40 mM NaClO<sub>4</sub> solution on Au/POAP electrodes was investigated. The results presented in the ESI† show no appreciable

variations in the contact angle values when changing  $V_g$  between  $-0.2$  and  $0.4$  V (Fig. S7†). These results suggest that the interaction between the charged surface groups and the mobile ions is the main mechanism implicated in the voltage-gated ionic transport of the PET/Au/POAP nanofluidic system.

As is shown from the results in Fig. 4, the system displayed a good tuning of ionic transport behavior by the application of low  $V_g$  ( $-0.2$  V  $< V_g < 0.4$  V). To test the reversibility of the iontronic response triggered by changes in the redox state of POAP, consecutive experiment switching  $V_g$  between  $-0.2$  V and  $0.4$  V was carried out. These  $V_g$  values were selected from the voltammetric response of POAP in this electrolyte solution and the iontronic behavior shown in Fig. 4, to guarantee the polymer film to be in its reduced (high rectification state) or oxidized form (low rectification state), avoiding the possible interference of any parasite electrochemical reaction (dissolved oxygen reduction or hydrogen evolution) or polymer overoxidation at lower or higher potential limits, respectively. Fig. 5(a) shows the switching of the iontronic output in terms of  $f_{\text{rec}}$ . These changes are related to a reversible transition between the reduced (red circles) and oxidized states (blue circles) of POAP. In agreement with the trend shown in Fig. 4, the application of a  $V_g = -0.2$  V produced the reduction of POAP in the nanochannel tip that caused an increase in the anion-driven rectification. The switching performance in terms of the iontronic current is presented in Fig. 5(b) and (c). Thus, the electrochemical reduction of POAP causes a current increment at  $V_t = 1$  V (high conductance state) and a decrease at  $V_t = -1$  V (low conductance state), which is responsible for a more marked diode-like asymmetry of the iontronic response.

In terms of real-world applications, a fast switching of the iontronic response after changing  $V_g$  is desirable. For this

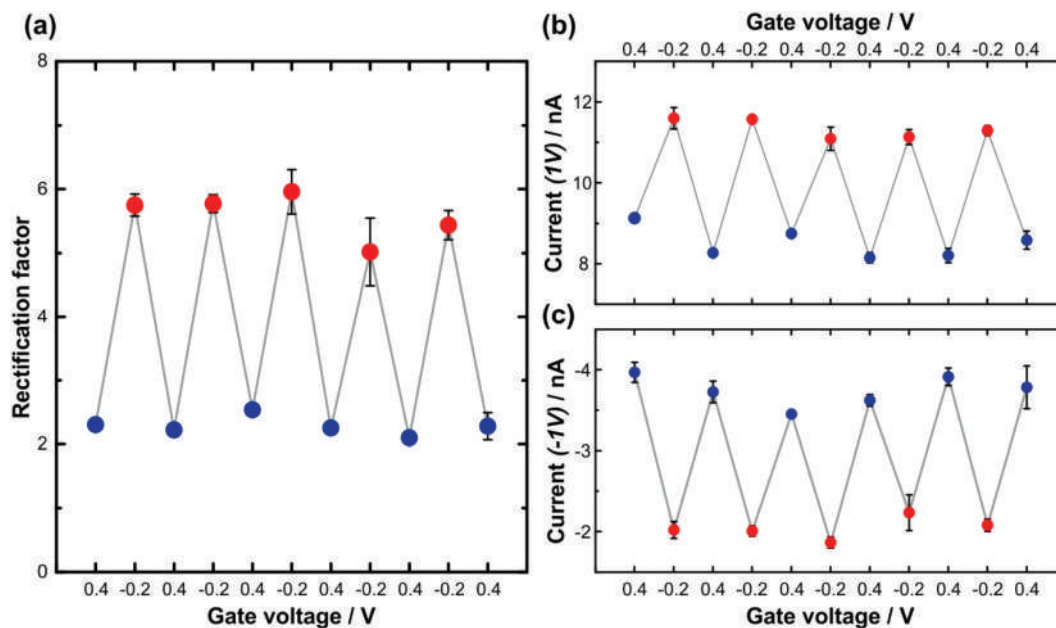
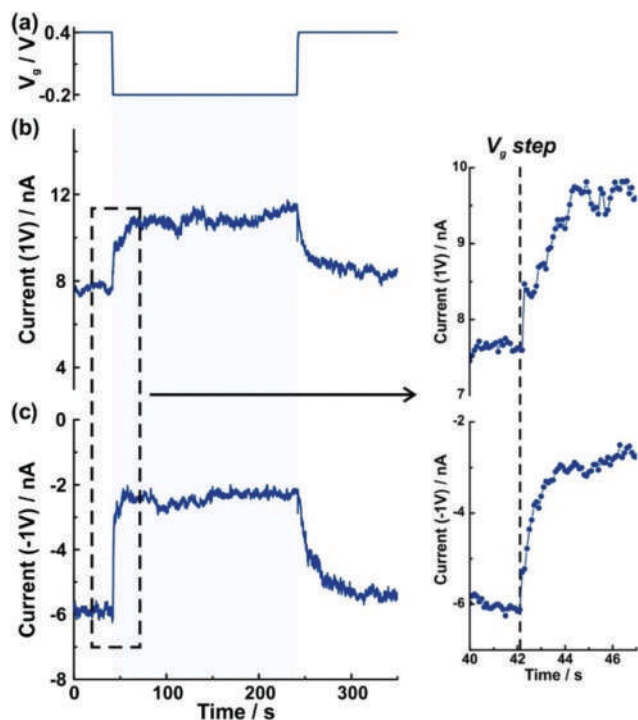


Fig. 5 Reversibility tests in terms of: (a) rectification factor, (b) current at  $V_t = +1$  V and (c) current at  $V_t = -1$  V. All measurements were carried out in a 10 mM HClO<sub>4</sub> + 40 mM NaClO<sub>4</sub> solution.



**Fig. 6** Left panel: (a) Gate voltage program used to study the dynamics of the device. Variations in the transmembrane current at (b)  $V_t = +1$  V and (c)  $V_t = -1$  V; right panel: zoom-in of the transition region. All measurements were carried out in a 10 mM  $\text{HClO}_4$  + 40 mM  $\text{NaClO}_4$  solution. (b) and (c) were obtained in different experiments with the same nanochannel and  $V_g$  programme.

reason, the dynamics of the ionic current after  $V_g$  perturbations were evaluated (Fig. 6). For this purpose, we recorded the ionic current at both 1 V and  $-1$  V using a four-electrode array and, simultaneously, a  $V_g$  programme employing a three-electrode array was applied. Fig. 6(a) shows the  $V_g$  steps used and Fig. 6(b) and (c) illustrate the ionic current switching at  $V_t = 1$  V and  $V_t = -1$  V, respectively. The zoom-in shows the quick iontronic output dynamics of the nFET. This feature is desirable for the rational design and development of nanochannels with a  $V_g$ -modulated selectivity.

## Conclusions

In summary, a nanofluidic field-effect transistor (nFET) based on the integration of the electroactive polymer POAP to SSNs was presented. This device allowed the precise control of ionic transport *via* the handling of a non-invasive stimulus as it is the gate voltage,  $V_g$ . Firstly, the tip of a bullet-shaped PET nanochannel fabricated by ion-track-etching was coated with Au and subsequently modified with POAP by electropolymerization. An interesting feature of the modification method is that it allows a fine control on the final tip diameter by managing the number of electropolymerization cycles. Furthermore, the application of different bias potentials  $V_g$  to the polymer film enabled the control of the POAP redox state and, conse-

quently, the nanochannel surface charge. More specifically, precise control in the iontronic output by means of the application of low  $V_g$  ( $<|0.2|$  V) was achieved. In this regard, the present system exhibited good reversibility with a quick and reliable response to the switching of  $V_g$ .

This work is a new example of the high potential of nFETs based on the integration of electroactive polymers to nanofluidic devices. The versatility of electroactive polymers added to the fascinating properties of SSNs can be a simple way for phasing up the development of devices with applications in fields such as filtration and nanoelectronics. Nanofluidic field-effect transistors constitute an emerging field and further studies are necessary to explore their potentialities and definite applications.

## Experimental section

### Materials

Monomer *o*-amino-phenol (*o*-AP) was purchased from Fluka. Perchloric acid and sodium hydroxide were of analytical grade. All reagents were used without further purification.

### Etching procedure

12  $\mu\text{m}$  thick PET foils were irradiated with a single swift heavy ion ( $\sim 2$  GeV Au) using a UNILAC linear accelerator of GSI Helmholtzzentrum für Schwerionenforschung. The damage induced to the material along the ion trajectory was removed by selective chemical etching, thus converting the ion track in a bullet-shaped nanochannel.<sup>50</sup> The etching procedure was performed in a home-made cell where one compartment was filled with 6 M NaOH at 60 °C for 7–8 min while the other side contained 6 M NaOH plus a small amount of anionic surfactant Dowfax 2a1 (0.05%). After etching, membranes were rinsed several times with Milli-Q water (18.2 M $\Omega$  cm at 25 °C) and also stored in water.

### Au deposition

A gold thin film ( $\sim 80$  nm) was deposited onto the tip side of PET foils (PET/Au) by sputtering as described previously.<sup>32</sup> The Au layer was used as the working electrode for electropolymerization.

### Electrochemical synthesis of POAP

3 mg of *o*-AP were dissolved in 10 ml of  $\text{HClO}_4$  0.1/ $\text{NaClO}_4$  0.4 M solution. POAP polymerization over the PET/Au foil was performed in a home-made conductivity cell (Fig. S3†) by cycling the potential between  $-0.25$  and  $0.8$  V at a scan rate of  $100$  mV  $\text{s}^{-1}$ .

### Spectroscopic measurements

Raman spectra were obtained with a BWTek Raman spectrometer (BWS415-532S) equipped with an optical microscope (BAC151B model). The excitation wavelength was 532 nm and the laser was focused on the sample using a 20 $\times$  optical magnification. Laser power was held at 50 mW. Spectra were recorded in the region of 100 to 4000  $\text{cm}^{-1}$ .

### Conductometric measurements

A bipotentiostat setup constituted of two potentiostats (Reference 600, Gamry Instruments) was used to apply both transmembrane and gate voltages independently. One of the potentiostats was used to measure the current–voltage (iontronic output) curves of the nanochannel (four-electrode configuration) and the other one was simultaneously used to apply different gate voltages using a typical three-electrode configuration. A detailed scheme of the experimental setup used for the field-effect measurements is shown in the ESI (Fig. S3†).

### Conflicts of interest

There are no conflicts to declare.

### Acknowledgements

G. L., V. M. C. and Y. T. T. acknowledge a scholarship from CONICET. M. L. C., W. A. M. and O. A. are CONICET fellows and acknowledge financial support from Universidad Nacional de La Plata (PPID-X016), CONICET (PIP-0370) and ANPCyT (PICT-2017-1523 and PICT2016-1680). C. T. and M. E. T. M. acknowledge support from the LOEWE project iNAPO funded by the Hessen State Ministry of Higher Education, Research and Arts. The irradiated PET foils are part of the experiment UMAT, which was performed at the beam line X0 at the GSI Helmholtzzentrum fuer Schwerionenforschung, Darmstadt (Germany) in the frame of FAIR Phase-0.

### References

- 1 B. Hille, *Ion Channels of Excitable Membranes*, Oxford University Press, 3rd edn, 2001.
- 2 Z. S. Siwy and S. Howorka, *Chem. Soc. Rev.*, 2010, **39**, 1115–1132.
- 3 K. Xiao, L. Wen and L. Jiang, *Small*, 2016, **12**, 2810–2831.
- 4 G. Pérez-Mitta, A. G. Albasa, C. Trautmann, M. E. Toimil-Molares and O. Azzaroni, *Chem. Sci.*, 2017, **8**, 890–913.
- 5 X. Hou, W. Guo and L. Jiang, *Chem. Soc. Rev.*, 2011, **40**, 2385.
- 6 G. Pérez-Mitta, M. E. Toimil-Molares, C. Trautmann, W. A. Marmisollé and O. Azzaroni, *Adv. Mater.*, 2019, 1901483.
- 7 R. Spohr, *Ion Tracks and Microtechnology: Principles and Applications*, Vieweg+Teubner Verlag, 1st edn, 1990.
- 8 X. Hou, H. Zhang and L. Jiang, *Angew. Chem., Int. Ed.*, 2012, **51**, 5296–5307.
- 9 I. Vlassioug, S. Smirnov and Z. Siwy, *Nano Lett.*, 2008, **8**, 1978–1985.
- 10 P. Y. Apel, Y. E. Korchev, Z. Siwy, R. Spohr and M. Yoshida, *Nucl. Instrum. Methods Phys. Res., Sect. B*, 2001, **184**, 337–346.
- 11 B. Schiedt, K. Healy, A. P. Morrison, R. Neumann and Z. Siwy, *Nucl. Instrum. Methods Phys. Res., Sect. B*, 2005, **236**, 109–116.
- 12 K. Xiao, P. Li, G. Xie, Z. Zhang, L. Wen and L. Jiang, *RSC Adv.*, 2016, **6**, 55064–55070.
- 13 H. Zhang, X. Hou, J. Hou, L. Zeng, Y. Tian, L. Li and L. Jiang, *Adv. Funct. Mater.*, 2015, **25**, 1102–1110.
- 14 Z. S. Siwy, *Adv. Funct. Mater.*, 2006, **16**, 735–746.
- 15 G. Pérez-Mitta, A. S. Peinetti, M. L. Cortez, M. E. Toimil-Molares, C. Trautmann and O. Azzaroni, *Nano Lett.*, 2018, **18**, 3303–3310.
- 16 B. Niu, K. Xiao, X. Huang, Z. Zhang, X.-Y. Kong, Z. Wang, L. Wen and L. Jiang, *ACS Appl. Mater. Interfaces*, 2018, **10**, 22632–22639.
- 17 K. Xiao, L. Chen, Z. Zhang, G. Xie, P. Li, X. Y. Kong, L. Wen and L. Jiang, *Angew. Chem., Int. Ed.*, 2017, **56**, 8168–8172.
- 18 S. Prakash, H. A. Zambrano, M. Fuest, C. Boone, E. Rosenthal-Kim, N. Vasquez and A. T. Conlisk, *Microfluid. Nanofluid.*, 2015, **19**, 1455–1464.
- 19 P. Li, G. Xie, X. Y. Kong, Z. Zhang, K. Xiao, L. Wen and L. Jiang, *Angew. Chem., Int. Ed.*, 2016, **55**, 15637–15641.
- 20 Y.-B. Zheng, S. Zhao, S.-H. Cao, S.-L. Cai, X.-H. Cai and Y.-Q. Li, *Nanoscale*, 2017, **9**, 433–439.
- 21 G. Pérez-Mitta, W. A. Marmisolle, L. Burr, M. E. Toimil-Molares, C. Trautmann and O. Azzaroni, *Small*, 2018, **1703144**, 1703144.
- 22 B. Yameen, M. Ali, R. Neumann, W. Ensinger, W. Knoll and O. Azzaroni, *Small*, 2009, **5**, 1287–1291.
- 23 S. Prakash and A. T. Conlisk, *Lab Chip*, 2016, **16**, 3855–3865.
- 24 W. Guan, S. X. Li and M. A. Reed, *Nanotechnology*, 2014, **25**, 122001.
- 25 C. Cheng, G. Jiang, G. P. Simon, J. Z. Liu and D. Li, *Nat. Nanotechnol.*, 2018, **13**, 685–690.
- 26 Y. Gogotsi, *Nat. Nanotechnol.*, 2018, **13**, 625–627.
- 27 K.-G. Zhou, K. S. Vasu, C. T. Cherian, M. Neek-Amal, J. C. Zhang, H. Ghorbanfekr-Kalashami, K. Huang, O. P. Marshall, V. G. Kravets, J. Abraham, Y. Su, A. N. Grigorenko, A. Pratt, A. K. Geim, F. M. Peeters, K. S. Novoselov and R. R. Nair, *Nature*, 2018, **559**, 236–240.
- 28 Y. Wang, H. Zhang, Y. Kang, Y. Zhu, G. P. Simon and H. Wang, *ACS Nano*, 2019, **13**, 11793–11799.
- 29 C. R. Martin, M. Nishizawa, K. Jirage, M. Kang and S. B. Lee, *Adv. Mater.*, 2001, **13**, 1351–1362.
- 30 E. B. Kalman, O. Sudre, I. Vlassioug and Z. S. Siwy, *Anal. Bioanal. Chem.*, 2009, **394**, 413–419.
- 31 G. Pérez-Mitta, W. A. Marmisollé, C. Trautmann, M. E. Toimil-Molares and O. Azzaroni, *Adv. Mater.*, 2017, **1700972**, 1–6.
- 32 G. Pérez-Mitta, W. A. Marmisollé, C. Trautmann, M. E. Toimil-Molares and O. Azzaroni, *J. Am. Chem. Soc.*, 2015, **137**, 15382–15385.
- 33 G. Laucirica, W. A. Marmisollé, M. E. Toimil-Molares, C. Trautmann and O. Azzaroni, *ACS Appl. Mater. Interfaces*, 2019, **11**, 30001–30009.

- 34 Q. Zhang, J. Kang, Z. Xie, X. Diao, Z. Liu and J. Zhai, *Adv. Mater.*, 2017, **1703323**, 1–7.
- 35 Q. Zhang, Z. Zhang, H. Zhou, Z. Xie, L. Wen, Z. Liu, J. Zhai and X. Diao, *Nano Res.*, 2017, **10**, 3715–3725.
- 36 R. Ren, Y. Zhang, B. P. Nadappuram, B. Akpınar, D. Klenerman, A. P. Ivanov, J. B. Edel and Y. Korchev, *Nat. Commun.*, 2017, **8**, 586.
- 37 G. Inzelt, *Conducting Polymers: A New Era in Electrochemistry*, Springer-Verlag Berlin Heidelberg, 2008.
- 38 M. E. G. Lyons, *Electroactive Polymer Electrochemistry*, Springer US, Boston, MA, 1st edn, 1994.
- 39 E. M. Geniès, A. Boyle, M. Lapkowski and C. Tsintavis, *Synth. Met.*, 1990, **36**, 139–182.
- 40 Z. H. Wang, C. Li, E. M. Scherr, A. G. MacDiarmid and A. J. Epstein, *Phys. Rev. Lett.*, 1991, **66**, 1745–1748.
- 41 C. Dhand, M. Das, M. Datta and B. D. Malhotra, *Biosens. Bioelectron.*, 2011, **26**, 2811–2821.
- 42 Q. Wu, Y. Xu, Z. Yao, A. Liu and G. Shi, *ACS Nano*, 2010, **4**, 1963–1970.
- 43 C. Barbero, J. Zerbino, L. Sereno and D. Posadas, *Electrochim. Acta*, 1987, **32**, 693–697.
- 44 W. A. Marmisollé, D. Gregurec, S. Moya and O. Azzaroni, *ChemElectroChem*, 2015, **2**, 2011–2019.
- 45 R. Tucceri, *Procedia Mater. Sci.*, 2015, **8**, 261–270.
- 46 R. Tucceri, *Poly(o-aminophenol) Film Electrodes: Synthesis, Transport Properties and Practical Applications*, Springer International Publishing, 1st edn, 2013.
- 47 T. Ohsaka, S. Kunitamura and N. Oyama, *Electrochim. Acta*, 1988, **33**, 639–645.
- 48 A. Guerrieri, R. Ciriello and D. Centonze, *Biosens. Bioelectron.*, 2009, **24**, 1550–1556.
- 49 W. Tao, D. Pan, Y. Liu, L. Nie and S. Yao, *Anal. Biochem.*, 2005, **338**, 332–340.
- 50 P. Y. Apel, I. V. Blonskaya, S. N. Dmitriev, O. L. Orelovitch, A. Presz and B. A. Sartowska, *Nanotechnology*, 2007, **18**, 305302.
- 51 C. Barbero, J. J. Silber and L. Sereno, *J. Electroanal. Chem.*, 1989, **263**, 333–352.
- 52 H. J. Salavagione, J. Arias, P. Garcés, E. Morallón, C. Barbero and J. L. Vázquez, *J. Electroanal. Chem.*, 2004, **565**, 375–383.
- 53 R. I. Tucceri, C. Barbero, J. J. Silber, L. Sereno and D. Posadas, *Electrochim. Acta*, 1997, **42**, 919–927.
- 54 J. M. Ortega, *Thin Solid Films*, 2000, **371**, 28–35.
- 55 H. J. Salavagione, J. Arias-Pardilla, J. M. Pérez, J. L. Vázquez, E. Morallón, M. C. Miras and C. Barbero, *J. Electroanal. Chem.*, 2005, **576**, 139–145.
- 56 G. Xie, P. Li, Z. Zhao, Z. Zhu, X.-Y. Y. Kong, Z. Zhang, K. Xiao, L. Wen and L. Jiang, *J. Am. Chem. Soc.*, 2018, **140**, 4552–4559.
- 57 M. R. Powell, L. Cleary, M. Davenport, K. J. Shea and Z. S. Siwy, *Nat. Nanotechnol.*, 2011, **6**, 798–802.
- 58 J. Cervera, B. Schiedt, R. Neumann, S. Mafé and P. Ramírez, *J. Chem. Phys.*, 2006, **124**, 104706.
- 59 C. Wei, A. J. Bard and S. W. Feldberg, *Anal. Chem.*, 1997, **69**, 4627–4633.
- 60 Z. Siwy, E. Heins, C. C. Harrell, P. Kohli and C. R. Martin, *J. Am. Chem. Soc.*, 2004, **126**, 10850–10851.
- 61 G. Laucirica, G. Pérez-Mitta, M. E. Toimil-Molares, C. Trautmann, W. A. Marmisollé and O. Azzaroni, *J. Phys. Chem. C*, 2019, **123**, 28997–29007.
- 62 Z. You-Yu, W. Mei-Ling, L. Mei-Ling, Y. Qin, X. Qing-Ji and Y. Shou-Zhuo, *Chin. J. Anal. Chem.*, 2007, **35**, 685–690.
- 63 M. E. Carbone, R. Ciriello, S. Granafèi, A. Guerrieri and A. M. Salvi, *Electrochim. Acta*, 2015, **176**, 926–940.
- 64 T. Komura, Y. Ito and K. Takahashi, *Electrochim. Acta*, 1998, **43**, 723.
- 65 S. Kunitamura, T. Ohsaka and N. Oyama, *Macromolecules*, 1988, **21**, 894–900.
- 66 C. Barbero, J. J. Silber and L. Sereno, *J. Electroanal. Chem. Interfacial Electrochem.*, 1990, **291**, 81–101.
- 67 J. Wang, M. Zhang, J. Zhai and L. Jiang, *Phys. Chem. Chem. Phys.*, 2014, **16**, 23–32.
- 68 Z. Siwy and A. Fuliński, *Phys. Rev. Lett.*, 2002, **89**, 4–7.
- 69 A. Fuliński, I. Kosińska and Z. Siwy, *New J. Phys.*, 2005, **7**, 132.
- 70 P. Y. Apel, I. V. Blonskaya, O. L. Orelovitch, P. Ramirez and B. A. Sartowska, *Nanotechnology*, 2011, **22**, 1–13.
- 71 P. Ramírez, P. Y. Apel, J. Cervera and S. Mafé, *Nanotechnology*, 2008, **19**, 315707.
- 72 G. Pérez-Mitta, A. Albesa, F. M. Gilles, M. E. Toimil-Molares, C. Trautmann and O. Azzaroni, *J. Phys. Chem. C*, 2017, **121**, 9070–9076.
- 73 Z. Zhang, L. Wen and L. Jiang, *Chem. Soc. Rev.*, 2018, **47**, 322–356.
- 74 M. Ali, B. Yameen, J. Cervera, P. Ramírez, R. Neumann, W. Ensinger, W. Knoll, O. Azzaroni, P. Ramı, R. Neumann, W. Ensinger, W. Knoll and O. Azzaroni, *J. Am. Chem. Soc.*, 2010, **132**, 8338–8348.
- 75 R. I. Tucceri, *J. Electroanal. Chem.*, 2003, **543**, 61–71.